Nanoscale Chemical Interaction Enhances the Physical Properties of Bioglass Composites

Roya Ravarian,[†] Xia Zhong,[†] Mike Barbeck,[‡] Shahram Ghanaati,[‡] Charles James Kirkpatrick,[‡] Ciara M. Murphy,[§,⊥] Aaron Schindeler,[§,⊥] Wojciech Chrzanowski,[∥] and Fariba Dehghani[†,*]

[†]School of Chemical and Biomolecular Engineering, The University of Sydney, Sydney, NSW, Australia, [‡]Institute of Pathology, University Medical Center of the Johannes Gutenberg University, Mainz, Germany, [§]Orthopaedic Research & Biotechnology Unit, The Children's Hospital at Westmead, Sydney, Australia, [⊥]Discipline of Paediatrics and Child Health, Faculty of Medicine, The University of Sydney, Sydney, Australia, and [∥]Faculty of Pharmacy, The University of Sydney, Sydney, NSW, Australia

ABSTRACT Bioglasses are favorable biomaterials for bone tissue engineering; however, their applications are limited due to their brittleness. In addition, the early failure in the interface is a common problem of composites of bioglass and a polymer with high mechanical strength. This effect is due to the phase separation, nonhomogeneous mixture, nonuniform mechanical strength, and different degradation properties of two compounds. To address these issues, in this study a nanoscale interaction between poly(methyl methacrylate) (PMMA) and bioactive glass was formed *via* silane coupling agent (3-trimethoxysilyl)propyl methacrylate (MPMA). A monolith was produced at optimum composition from this hybrid by the sol–gel method at 50 °C with a rapid gelation time (<50 min) that possessed superior physicochemical properties compared to pure bioglass and physical mixture. For instance, the Young's modulus of bioglass was decreased 40-fold and the dissolution rate of silica was retarded 1.5-fold by integration of PMMA. Prolonged dissolution of silica fosters bone integration due to the continuous dissolution of bioactive silica. The primary osteoblast cells were well anchored and cell migration was observed on the surface of the hybrid. The *in vivo* studies in mice demonstrated that the integrity of the hybrids was maintained in subcutaneous implantation. They induced mainly a mononuclear phagocytic tissue reaction with a low level of inflammation, while bioglass provoked a tissue reaction with TRAP-positive multinucleated giant cells. These results demonstrated that the presence of a nanoscale interaction between bioglass and PMMA affects the properties of bioglass and broadens its potential applications for bone replacement.

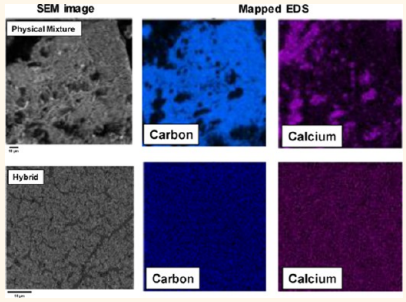

KEYWORDS: hybrids · PMMA · bioglass · sol–gel · bone regenerative material · nanocomposites

Bioceramics such as bioglass are favorable materials for bone grafting applications due to the high biocompatibility and bonding capability to the host tissue in the body.[1−6] The surface of bioactive materials forms a biologically active hydroxyapatite layer, which provides the bonding interface with tissues. This apatite phase is chemically and structurally equivalent to the mineral phase in bone, providing interfacial bonding.[7] Among bioceramics, silica-based materials show great potential for bone tissue regeneration applications. One of the major obstacles for the application of bioglass in bone repair is its poor mechanical properties, which make its manufacturing a challenging issue. Several attempts have been made to resolve the issues associated with the brittle and fragile structure of bioglass prior to bone grafting.[8] Introducing materials with a lower elastic modulus such as polymer matrices is a strategy to improve the mechanical properties of bioglass and mimic the natural bone structure.[9−11]

Poly(methyl methacrylate) (PMMA) is a synthetic polymer often used to augment the mechanical properties of bioglass.[8,11−15] This polymer has broad biomedical applications due to its self-hardening property and excellent mechanical properties.[16] It has been used for prosthetic fixation, as a bone substitute in orthopedics, and as a self-curing reagent in dental prosthetics.[17,18] PMMA-based bone cements were first introduced in 1960s.[19] Since then, progress has been made to improve their properties for fixation of implants and filling bone voids after removal of tumors or trauma.[13] For example, in orthopedic and dentistry operations, a mixture of methyl methacrylate

* Address correspondence to Fariba.dehghani@sydney.edu.au.

Received for review April 30, 2013 and accepted September 3, 2013.

Published online September 03, 2013
10.1021/nn402157n

(MMA) monomer, initiators, and activators is placed in the body, and the fixation occurs by *in situ* polymerization.[20] This approach, however, is not desirable due to several issues including damage to the surrounding tissues as a result of temperature raise (70 °C) from an exothermic reaction; release of toxic compounds such as residual MMA monomer, initiators, and activators; and inertness and lack of bioactivity. These issues lead to the thickening of an intervening fibrous tissue layer; inhibition of cell function and growth/differentiation; increased inflammatory response and cell death/necrosis; and finally loosening of prosthesis/implants.[11,13,21] Several approaches have been attempted to resolve the problems of PMMA-based implants. For example, the amount of MMA monomer was reduced with the addition of PMMA polymer to the mixture. This reduced the heat generation during the exothermic reaction, minimizing the damage to surrounding tissues.[22−24] However, this method still does not eradicate the issue of adding MMA monomer for *in situ* polymerization and low bioactivity.

Bioglass powder was added as a filler to PMMA-based biomaterials to enhance their biocompatibility and bioactivity.[13,14,23,25] The amount and particle size of bioglass powder have a significant effect on the bioactivity of PMMA−bioglass physically mixed composites. Decreasing the particle size of bioglass increases the surface area, resulting in higher exposure of bioactive compounds to the surrounding tissue, hence enhancing the bioactivity of the implant.[12,23,26] However, physical mixtures of PMMA and bioglass may be nonuniform due to the lack of adhesion between these two materials and the absence of molecular interaction.

Phase separation is a challenging issue in manufacturing ceramic−polymer composites (physical mixtures) due to the different inherent physicochemical characteristics of these two compounds. This effect leads to the formation of cavities in their interfaces and sudden changes in the structural properties of the material.[27,28] Discrepancies in the physical properties, such as degradation rate and mechanical strength, increase the risk of implant failure.[12,29] Additionally a UV- or photosensitive initiator may be added to the composite for *in situ* polymerization of MMA monomer to promote homogeneous mixing of these two compounds.[30] This strategy accelerates the gelation time of these composites, which is favorable for injectable bone implants. However, these reagents may be toxic to surrounding tissues.

Organic−inorganic hybrids have been introduced as an alternative approach to address the issue of phase separation in physical mixing.[31] The interaction between PMMA−bioglass ranges from weak van der Waals and hydrogen bondings (class I hybrid) to strong covalent bonds (class II hybrid). Organosilane coupling agents such as 3-(trimethoxysilyl)propyl methacrylate (MPMA), shown in Figure 1, are molecules with both organic and inorganic moieties that provide the active sites for covalent bonding between organic and inorganic molecules.[32] These hybrids are commonly produced by the sol−gel method at moderate temperatures, which is the favorable method for the incorporation of an organic compound into the structure of an inorganic substance without thermal degradation.[33] Furthermore, the sol−gel method is efficient in creating a homogeneous distribution between two phases as a result of dissolving both compounds in a common solvent. The presence of MPMA organosilane coupling agent results in the formation of Si−O−Si covalent bonds to the silica network and formation of a homogeneous mixture of PMMA−bioglass. The schematic molecular structures of PMMA, MPMA, and PMMA−bioglass are shown in Figure 1.

PMMA−silica hybrids have been used in optics,[34] mechanics,[34−36] and electronics.[36,37] Few studies synthesized and characterized the physical and chemical properties of PMMA−silica hybrids and introduced this material as a candidate for bone cements[38] and dental[39,40] applications. The bioactivity of PMMA−silica hybrids was confirmed by the formation of an apatite layer on the surface.[16,29] In comparison with pure PMMA polymer, the cell response was also promoted in samples containing silica.[41,42] However, these studies have not investigated the impact of covalent bonding at the molecular level on bioactivity, physicochemical, and biological properties of hybrids, which was one of the objectives for our study.

MPMA has been used as a coupling agent to enhance chemical bonding between bioglass and PMMA to fabricate hybrids with superior properties. It was perceived that MPMA composition has a negligible effect on the molecular interaction between PMMA−bioglass and formation of the hybrid.[43] However, we have previously demonstrated that the composition of MPMA has a significant impact on chemical conjugation between PMMA and silica and formation of homogeneous hybrids.[44] The hybrids produced from a 0.1 molar ratio of MPMA:MMA were transparent, underlining the absence of phase separation; however, at lower molar ratios (*i.e.*, 0.004, 0.02), samples were opaque due to phase separation between PMMA and bioglass. This observation was confirmed by the results of one- and two-dimensional solid-state NMR, indicating strong intermolecular interaction between bioglass and PMMA at a molecular level when using 0.1 molar ratio of MPMA:MMA, while at lower ratios this interaction was low.[44] Additionally, this nanoscale interaction shifted the degradation temperature of this hybrid fabricated at 0.1 molar ratio of MPMA:MMA to 400 °C, which was at least 10% higher than PMMA and hybrids prepared from MPMA:MMA < 0.1 (mol ratio).[43,44] The PMMA-*co*-MPMA produced at higher molar ratios of MPMA:MMA (*e.g.* >0.1) was very viscous and involved complicated purification steps. Therefore, a 0.1 MPMA:MMA molar ratio was deemed as the optimum composition for the fabrication

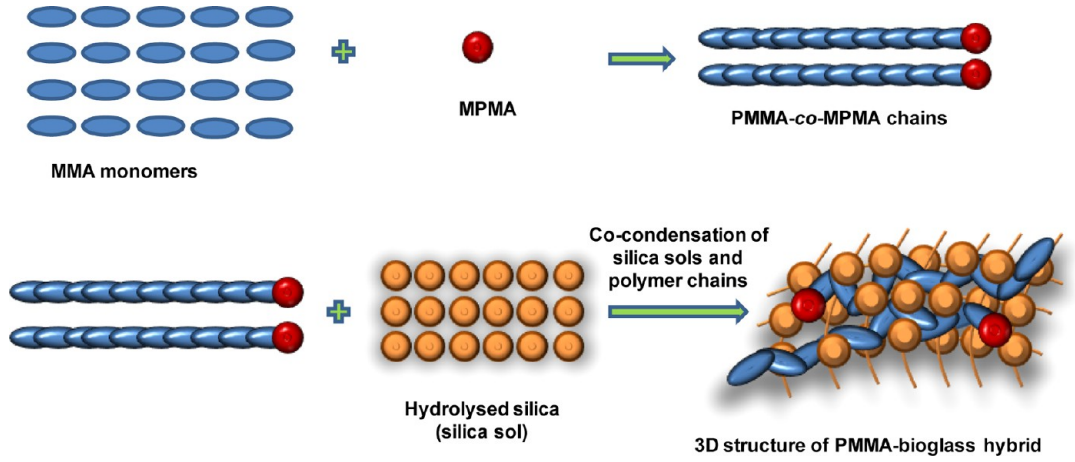

Figure 1. Schematic procedure for the fabrication of a PMMA–bioglass class II hybrid.

of bioglass–PMMA hybrids. It is important to note that it was viable to fabricate hybrids with various ratios of bioglass:PMMA when using a 0.1 MPMA:MMA molar ratio.

The morphology, mechanical properties, and degradation profiles are the crucial factors for bone implant applications. Therefore, in this study, we aim to investigate the effect of intermolecular interactions on the properties of PMMA–bioglass. A 0.1 MPMA:PMMA molar ratio was used to fabricate hybrids, and their properties were compared with a physical mixture and neat bioglass. Analytical methods such as scanning electron microscopy (SEM), energy dispersive spectrometry (EDS), atomic force microscopy (AFM), and scanning transmission electron microscopy (STEM) were used to investigate the surface properties of these composites. Furthermore, the effect of covalent bonding and molecular interaction of hybrids on the mechanical strength and degradation profile was assessed. Finally, *in vitro* and *in vivo* assays were conducted to compare the bioactivity, cell adhesion properties, and cytotoxicity of hybrids with bioglass and a physical mixture.

RESULTS AND DISCUSSION

In this study the physical properties of the hybrid (H1) were compared with the physical mixture of PMMA–bioglass (H0). Both pure bioglass and PMMA homopolymer were considered as control samples, as shown in Table 1. It was observed that only H1 formed a one-phase, transparent, three-dimensional (3D), monolith structure, which is due to the formation of covalent bonding between MPMA and silanol groups of bioglass.[44] However, in the absence of MPMA, the sol–gel method was not efficient for the creation of a uniform mixture of PMMA and bioglass, and two separate phases of a thin film of polymer and a gel structure of brittle bioglass were formed. Previous studies have shown that it is viable to create a 3D structure of PMMA–bioglass of different composition by *in situ* polymerization of MMA monomers in the presence of bioglass as a filler. However, these

TABLE 1. Optical Transparency and Gelation Time of Different Samples[a]

					gelation time (h)	
sample	MPMA:MMA (mol ratio)	M_n (Da), PDI	sol(B): sol(A)	optical transparency	25 °C	50 °C
H1	0.1		60:40	T	5	0.75 (45 min)
H0	0		60:40	NT	NG	NG
bioglass				T	120	3
PMMA	0	17025, 1.89			NG	NG
PMFS	0.1	21721, 1.77			NG	NG

[a] T: transparent; NT: not transparent; NG: no gel formation; M_n: number average molecular weight; PDI: polydispersity index; PMFS: functionalized PMMA using 0.1 molar ratio of MPMA:MMA.

products are still not as uniform as hybrids and exhibit a nonhomogenous degradation profile and nonuniform distribution of mechanical force due to the different load-bearing characteristics of polymer and bioglass particles.[45]

The hybrid and bioglass were formed within 5 and 120 h by the sol–gel method at room temperature, respectively. However, it was found that by increasing the temperature from 25 °C to 50 °C the gelation times of H1 and bioglass were decreased dramatically to 3 h and 45 min, respectively. These data demonstrate the significant impact of temperature on the formation of a silica network.[46,47] The faster gelation of H1 compared to bioglass was due to the presence of strong Si–C bonds.[46,48] Rapid gelation is favorable for the fabrication of *in situ* products in clinical applications.

Morphological Analyses. The morphology of H0 and H1 was compared in the macro- and nanoscale to assess the risk of phase separation as a result of lack of molecular integration. As shown in Figure 2, the differences in surface characteristic of bioglass (Figure 2a) and H0 (Figure 2b) elucidate the appearance of phase separation between ceramic and polymer for the physical mixture of PMMA and bioglass (H0). However, the surface of hybrid samples in Figure 2(c) was homogeneous, and

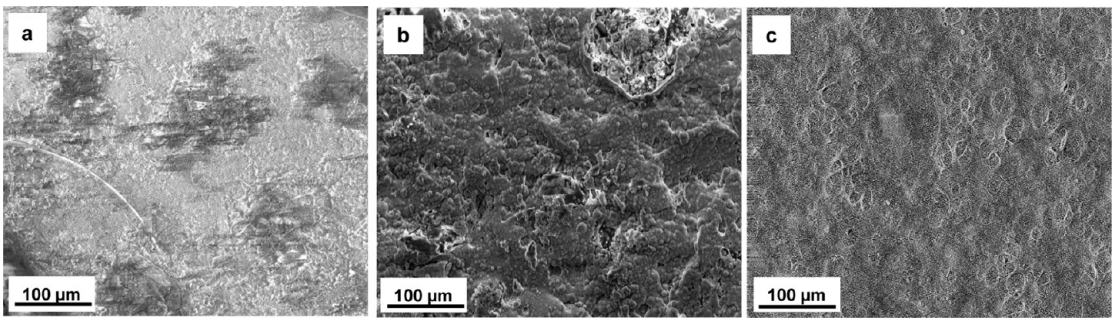

Figure 2. SEM images of (a) bioglass, (b) H0, and (c) H1.

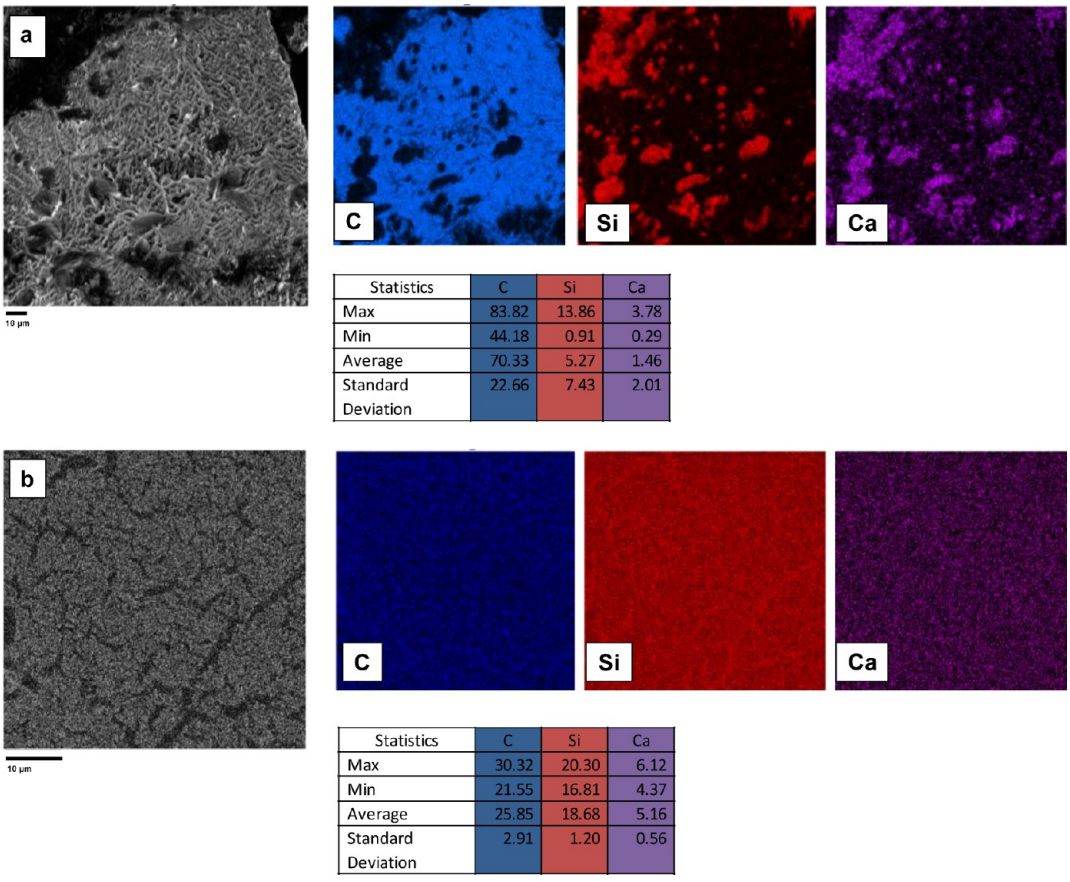

Statistics	C	Si	Ca
Max	83.82	13.86	3.78
Min	44.18	0.91	0.29
Average	70.33	5.27	1.46
Standard Deviation	22.66	7.43	2.01

Statistics	C	Si	Ca
Max	30.32	20.30	6.12
Min	21.55	16.81	4.37
Average	25.85	18.68	5.16
Standard Deviation	2.91	1.20	0.56

Figure 3. EDS results of (a) H0 and (b) H1 including the EDS mapping results for carbon, silicon, and calcium elements and the statistical results of the presence of elements.

no phase separation occurred in the structure of H1, underlining the presence of chemical conjugation resulting in structural integrity. The absence of phase separation in H1 and a homogeneous distribution of bioglass in the PMMA structure was further confirmed by mapping the SEM image by an EDS detector. The results in Figure 3 and quantitative analysis of these data demonstrated that calcium, silicon, and carbon were distributed uniformly throughout the H1 sample, while for H0, calcium was detected only on a few regions of the surface. The absence of phase separation in nanoscale for H1 and formation of two phases for H0 were elucidated by STEM analysis, as shown in Figure 4.

AFM analysis was used to compare the surface properties of hybrids fabricated in this study with a physical mixture of PMMA–bioglass. The roughness values were nonuniform for the H0 sample, underlining the nonhomogenous distribution of applied stress. However, as depicted in Figure 5, the surface of the H1 hybrid was smoother and the roughness dropped 5-fold compared to the physical mixture.

The results of analysis by SEM, EDS, STEM, and AFM demonstrated that the addition of a 0.1 molar ratio of MPMA:MMA that led to covalent bonding between PMMA and bioglass was efficient in creating a homogeneous mixture of PMMA and bioglass. This amount of coupling

agent was adequate to prevent phase separation between these two organic and inorganic phases.

Mechanical Properties. Mechanical properties are one of the key factors for selecting a biomaterial.[43] The bulk mechanical properties of prepared hybrid monoliths were compared to neat bioglass (BG). The physical mixture (H0) was excluded from this test due to the lack of 3D structure and nonuniform gel formation. As shown in Figure 6(a), the uniaxial stress−strain compression curves of H1 and BG showed two regions (I and II) before fracture: the linear region I, from which the Young's modulus was calculated, and the quasi-linear region, in which the stress was increased until fracture. It was observed that region I in H1 extended up to 0.1 mm/mm, while this region was decreased 10-fold in BG and did not exceed 0.01 mm/mm. Furthermore, the 40-fold reduction of the Young's modulus of bioglass (229 MPa) compared to H1 (6 MPa) resulted in achieving higher mechanical stability for the hybrid samples. The ultimate strain of H1, also, was 8-fold higher than the bioglass sample (Figure 6(b)), which completely collapsed in the first stage of the mechanical test. Moreover, the toughness of the hybrid was 2.6-fold higher than the bioglass sample. The enhancement of mechanical properties of H1 was attributed to the covalent bonding (Si−O−C bonds) and integration of PMMA chains into the silica structure.

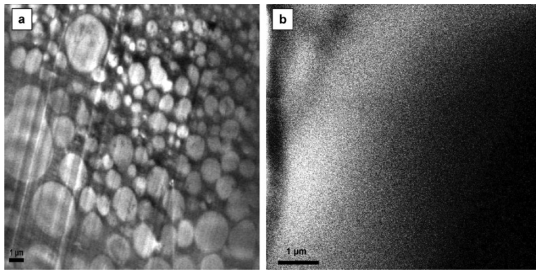

Figure 4. STEM images of (a) H0 and (b) H1.

It is favorable to develop a biomaterial that mimics the hardness of the host tissue.[49] As shown in Figure 6-(c), the hardness value of the H1 hybrid was close to natural bone (*i.e.*, 33−45 Vickers hardness (HV))[50] and significantly higher than bioglass and PMMA and even their physical mixtures ($p < 0.001$). These data demonstrated that H1 was more stable and less deformed under stress compared to H0, bioglass, and PMMA. It can be concluded that the integration of PMMA chains into the molecular structure of silica increased the toughness and ductility, while decreasing the brittleness. The compression strength and Young's modulus of the H1 that was prepared from 60:40 vol % PMFS:bioglass solutions were within the range suitable for osteoblast cell adhesion and proliferation.[7,51,52] An *in vitro* cell study was then conducted to assess the cell adhesion to this material.

Degradation Analysis. One of the challenging issues in the application of composite materials is the separate degradation profile of each component, especially when one of the components degrades before the regeneration of the tissue.[12] Inhomogeneous degradation causes uneven stress distribution or load transmission on the composite materials that leads to adverse effects such as loosening of the implant.

The degradation of H1, bioglass, and pure PMMA samples was measured within 100 days. The data in

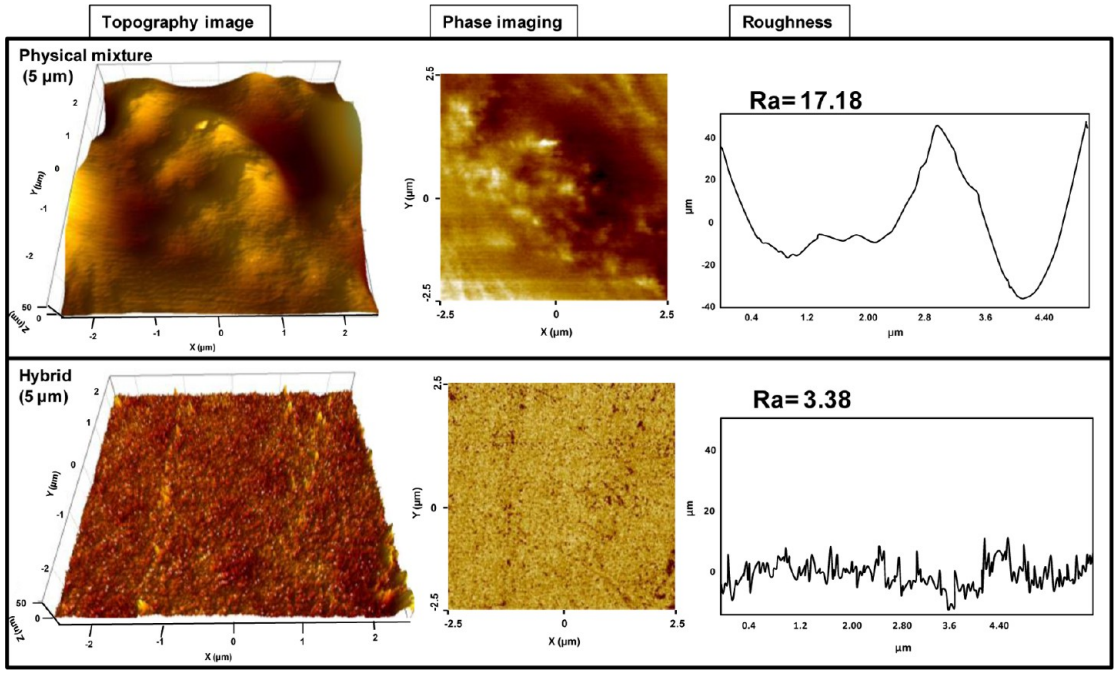

Figure 5. AFM results including topographic images, phase imaging, and roughness of the surface of H0 (physical mixture) and H1 (hybrid).

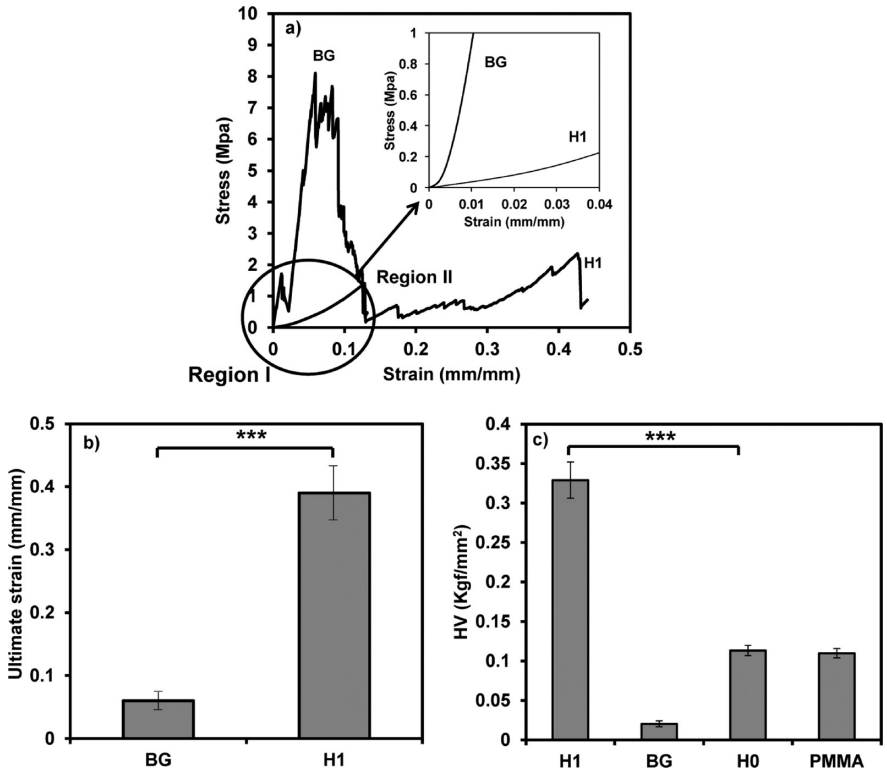

Figure 6. Mechanical properties of bioglass and H1 samples: (a) stress−strain diagram, (b) ultimate strain, (c) microhardness values (* represents $p < 0.001$).**

Figure 7 show that PMMA has no weight loss during this period; however, bioglass was rapidly degraded and completely dissolved after 83 days. The mechanism of degradation of bioglass is well established in the literature.[45,53−55] During the degradation of bioglass, SiO_2 is gradually dissolved and results in producing silicic acid, which is excreted from the body.[45,53−55] However, the degradation rate of SiO_2 matrices is a function of parameters such as the composition of precursors, water:TEOS molar ratio, pH, and network connectivity of the silica matrix that is shown by Q^n species.[56] Q^n shows the number of Si−O−Si bonds around each silicon. For example, the high value of Q^3 and low value of Q^4 are indicative of a less compact network and hence a faster degradation rate. Previous studies also showed that the covalent bonding between a bioglass and a polymer had a negligible effect on the mechanism of degradation that is based on releasing the silica ion.[45,57]

The composition of bioglass in this study was TEOS: water:HCl:CC = 1:8:0.01:0.2 with 41% Q^3 and 53% Q^4 species, which were calculated from ^{29}Si NMR analysis.[44] The data in Figure 7 demonstrated that these characteristics led to the degradation rate of 0.92% per day and 0.65% per day for bioglass and H1 samples, respectively. The zero-order kinetics of bioglass degradation was in agreement with other studies.[53] The addition of PMMA to bioglass by covalent bonding (H1) resulted in impeding the degradation rate of bioglass by 1.5-fold and maintaining nearly 30% of its original weight after 100 days of

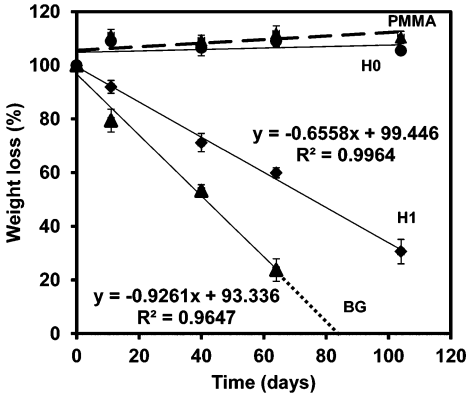

Figure 7. Degradation profiles of hybrid compared with pure PMMA and bioglass (the data were extrapolated for BG until day 83).

incubation. It was demonstrated that the mechanism of the new bone formation at the implant interface and the host tissue continues until there is ion exchange between the implant and body fluids.[58] Therefore, retarding the degradation of the silica matrix in H1 provides a longer period for ion exchange, hence resulting in stronger interaction with the host tissue and formation of thicker apatite for bone formation. It is assumed that during gradual degradation of bioactive glass innate hydroxyapatite and extracellular matrix are regenerated *in situ* that mimic the required mechanical strength for bone regeneration. In addition, no weight loss was observed in the degradation profile of H0, which was due to the fact that

the hydrophobic PMMA did not facilitate the interaction of bioglass particles with the surrounding solution.

The FTIR analysis conducted on the residues of the H1 sample after 100 days' incubation in PBS at 37 °C confirmed the presence of silica ions in the degraded H1 sample. As shown in Figure 8, C═O and CO_3^{2-} peaks of polymer and bioglass were detected at 1722 and 1625 cm^{-1}, respectively. The presence of the 1625 cm^{-1} peak in the solid residues underlines that after 100 days bioglass was still maintained in the solid phase and was not completely dissolved in the media. The ratio of intensities for characteristic peaks at 1625/1722 cm^{-1} was indicative of bioglass degradation. This ratio is calculated to change from 2 to 0.66 after degradation, which was in agreement with 67% weight loss of H1. This slower degradation rate is suitable for bone implant due to the fact that at least 90 days' implantation time is required for bone tissues to regenerate.[58] The visual observation and the presence of a strong peak at 1722 cm^{-1} confirmed the presence of PMMA in the degraded sample.

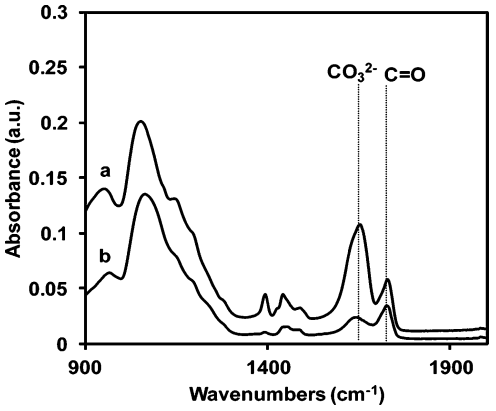

Figure 8. FTIR spectra of (a) H1 and (b) residues of degraded H1.

Biological Activity of PMMA–Bioglass Hybrids. Prior to *in vitro* testing, the bioactivity of the hybrid was tested by incubation of samples in simulated body fluid (SBF), which is a standard method for selection of biomaterials for bone and dental applications.[59–61] In this method, formation of an apatite layer is indicative of bioactivity of samples. As shown in Figure 9, an apatite layer was clearly observed on the surface of both bioglass and hybrid samples. On the other hand, no apatite layer was formed on the PMMA surface due to the inertness of this polymer. In the physical mixture (H0), formation of apatite was observed only in some regions of the surface, and full coverage similar to the hybrid was not detected. This result confirmed the formation of apatite only on the surface of bioglass. One of the main advantages of hybrids compared to physical mixtures or conventional composites is that the inorganic layer is well distributed over the surface and it is more accessible for precipitation and formation of a calcium-phosphate layer. However, in physical mixtures the organic phase covers the surface of samples and decreases the interface between the

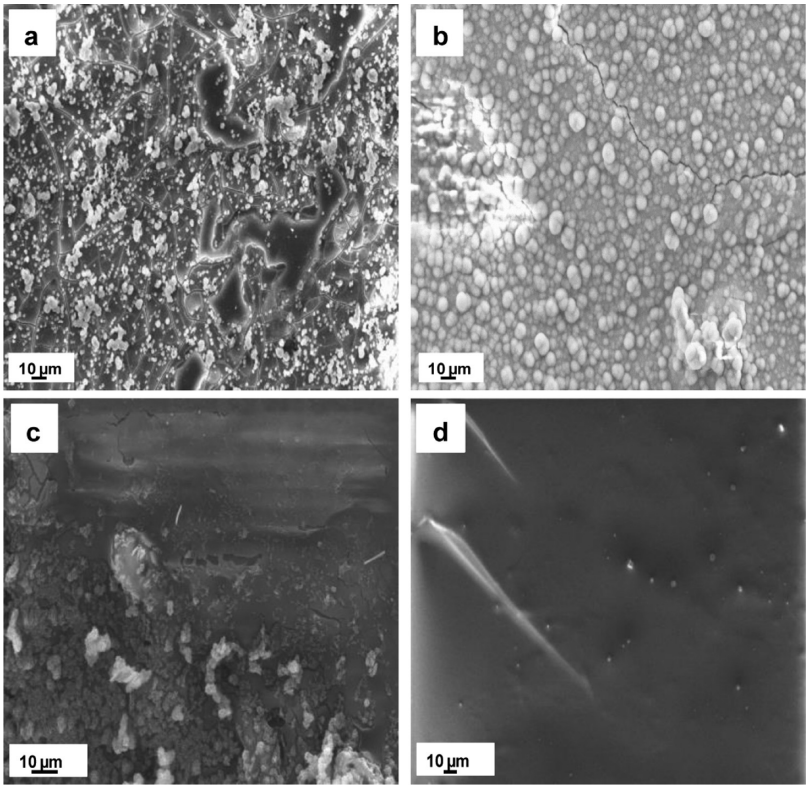

Figure 9. Bioactivity test shows the formation of HA on the surface of (a) bioglass, (b) H1, (c) H0, and (d) PMMA samples after 7 days' incubation in SBF.

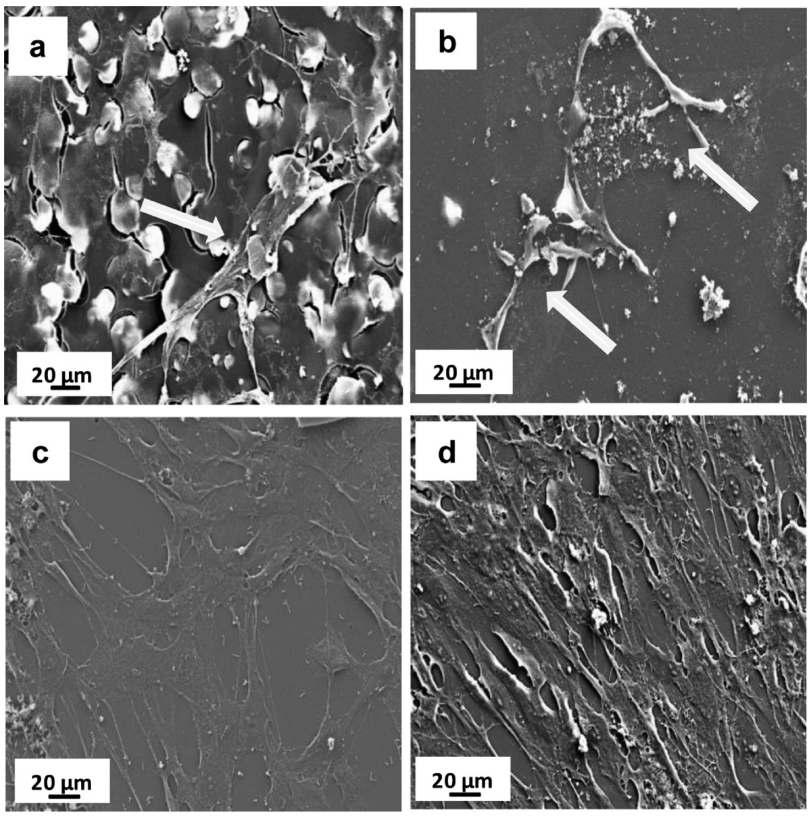

Figure 10. SEM images of (a) pure PMMA, (b) H0, (c) H1, and (d) bioglass. White arrows show the individual narrowed cells on the surface of samples.

inorganic phase and calcium-phosphate ions.[32] Furthermore, the formation of apatite on the surface of H1 implies that the presence of inert PMMA polymer with a composition of 60:40 PMFS:bioglass had a negligible impact on bioactivity.

***In Vitro* Attachment, Proliferation, and Osteoblastic Differentiation.** Physical mixture (H0) and hybrid (H1) of PMMA-bioglass were analyzed *in vitro* for their cell attachment and osteoblast growth properties. These materials were compared with their constituent materials, pure PMMA and bioglass. The bioglass was markedly brittle and prone to thermal and mechanical shock-induced fracturing.

Cells were found to adhere to all surfaces and supported attachment after 4 days in culture, as visualized by scanning electron microscopy (Figure 10). Cells showed a more flattened morphology, indicative of increased attachment on bioglass compared to PMMA. Notably this morphology was better maintained on the hybrid H1 compared to H0, suggesting the improved homogeneity of the PMFS-bioglass gave more consistent attachment.

Cell growth was measured by viability assay on cultured primary osteoblasts at days 1 and 7 after cell seeding. No significant difference was seen between the samples after 24 h; however the H1 hybrid showed a remarkable increase after 7 days, which was superior to all other samples including the physical mixture in terms of cell viability. The cell viability number of H1 was close to the control (TCPS) after 7 days of culture ($p > 0.05$). A trend toward increased viability was seen in tissue culture plastic controls, although this is a surface optimized for cell attachment and growth.

Finally, the alkaline phosphatase (ALP) activity of samples was assessed. Human preosteoblasts were grown on H0, H1, PMMA, and bioglass materials and treated with osteogenic differentiation media to induce expression of mature osteoblast markers. Robust staining was seen on cells grown on tissue culture plastic as a positive control (Figure 12). Notably, blue ALP+ cells were seen on the H1-treated hybrid samples but not on the H0 samples or on the PMMA or bioglass alone. These data suggest that the hybrid material may have superior properties as a bone replacement material for early osteoblast differentiation.

***In Vivo* Study.** *Histological Results: Bioglass Group.* The brittleness of bioglass resulted in the formation of bulk-like structures within the implantation bed and fragments of various sizes ranging up to small particles after 10 days. As shown in Figure 13 and Figure 14, the implantation of this material provoked two different cellular reactions. Around the bulk-like structures within the implantation bed granulocytes and mononuclear cells, mainly macrophages and lymphocytes, were

embedded within a well-vascularized granulation tissue (Figure 13(a)). The immunohistochemical detection of the macrophage-specific F4/80 antigen showed that these cells were mainly detectable as a monolayer at the material–tissue interface and loosely distributed within the material–adherent granulation tissue (Figure 13(b)). Furthermore, only a small percentage of cells within the peri-implant tissue was shown to express tartrate-resistant acid phosphatase (TRAP) (Figure 13(c)).

The tissue reaction to bioglass fragments was dominated by multinucleated giant cells in addition to the above-mentioned mononuclear cells (Figure 14(a,b)). The immunochemical detection of the F4/80 antigen additionally revealed the dominance of macrophages among all material-adherent mononuclear cells (Figure 14(b)). Furthermore, TRAP staining revealed that within the implantation bed of fragments both TRAP-positive mononuclear and multinucleated cells dominated when compared to those without TRAP expression (control samples)

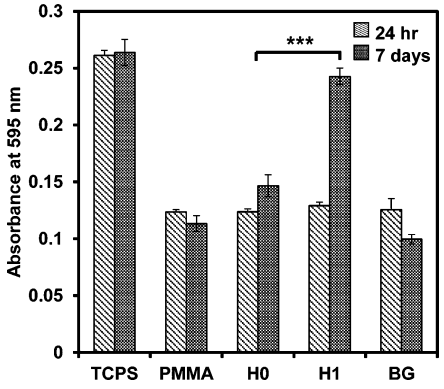

Figure 11. Viability assay of H1 hybrid sample compared to the PMMA and bioglass (* represents $p < 0.001$).**

(Figure 14(c)). We postulate that the occurrence of the multinucleated giant cells within the bioglass might be mainly size-related and less associated with the potential material impurity.

Histological Results: H1 Group. Better mechanical properties and less brittleness of H1 samples in comparison to the bioglass resulted in almost no material fragments within the peri-implant tissue during implantation and explantation (Figure 15). Thus, only one cellular reaction pattern was detected. The histological analysis at day 10 after implantation revealed that the H1 implant was embedded within a cell- and vessel-rich connective tissue (Figure 15). This tissue was localized as a relatively thick wall along the material–tissue interface and contained macrophages, granulocytes, and lymphocytes as well as fibroblasts. The tissue reaction was comparable to that toward the bioglass bulk-like structures. It should be noted that no cell and tissue penetration into the material core was observed due to the lack of porosity. Directly at the surface of the H1 implant predominantly macrophages were located (Figure 15). Furthermore, a fewer number of multinucleated cells was detectable within the tissue adjacent to the material (Figure 15(b)). TRAP detection revealed that only a small number of cells at the surface of the H1 implant showed expression of this enzyme (Figure 15(c)).

In this study an *in vivo* pilot study was performed in order to assess the tissue reaction to bioglass and H1 samples. The histological evaluation has revealed that during the implantation phase of 10 days bioglass underwent a fragmentation most likely due to physical forces during animal movement rather than tissue penetration into the material. Consequently, this

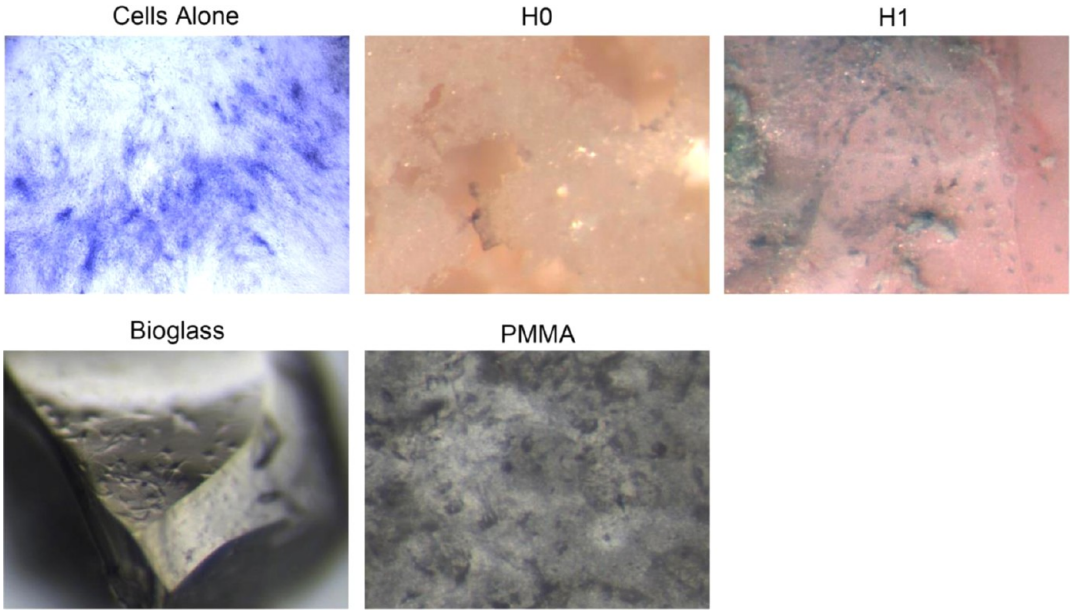

Figure 12. ALP staining on materials showing ALP+ cells (blue) after 4 days of osteogenic differentiation. Positive staining was seen on H1 hybrid and tissue culture plastic, but not on PMMA, bioglass, or H0 material.

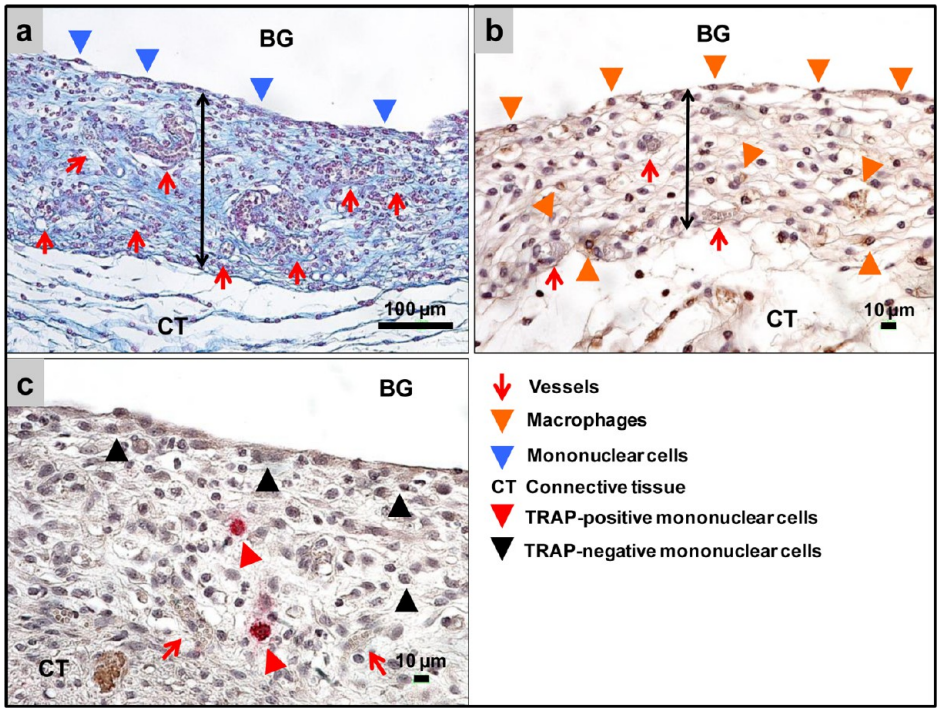

Figure 13. Tissue reaction to the bioglass implant at day 10 after implantation. (a) Azan-staining: the vessel-rich (red arrows) multilayered tissue wall (double arrow) covering the bulk-like structural segments of the implanted material (BG). A layer of mononuclear cells (blue arrowheads) was adherent to the material surface. (b) Macrophage-specific F4/80-immunostaining: macrophages (orange arrowsheads) were located in all regions of the peri-implant tissue (double arrow). (c) TRAP staining: only a low number of mononuclear cells within the peri-implant tissue expressed TRAP (red arrowheads), while the majority of these cells were TRAP-negative (black arrowheads).

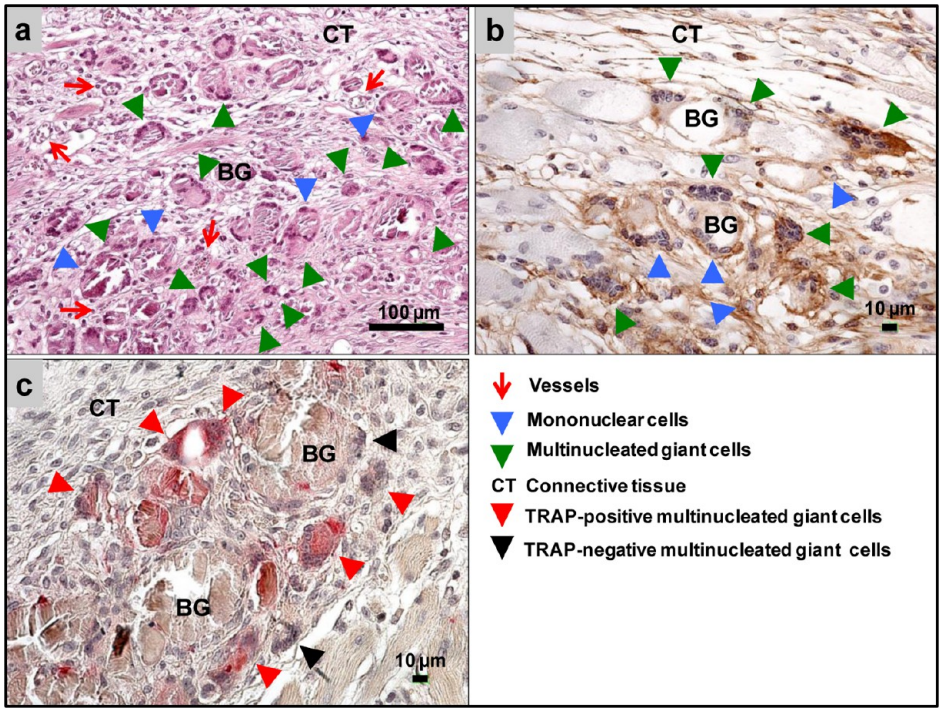

Figure 14. Tissue reaction to bioglass fragments at day 10 after implantation. (a) H&E staining: an overview of the implantation bed of fragments (BG), which were embedded within a vessel-rich (red arrows) granulation tissue. At their surfaces mononuclear (blue arrowheads) and multinucleated cells (green arrowheads) were observable. (b) Macrophage-specific F4/80-immunostaining: the involvement of phagocytic mono- and multinucleated cells (blue/green arrowheads) in the tissue reaction to the bioglass fragments (BG). (c) TRAP staining: the marked presence of multinucleated giant cells involved in the degradation of the bioglass fragments. These cells showed higher TRAP-enzyme expression potential.

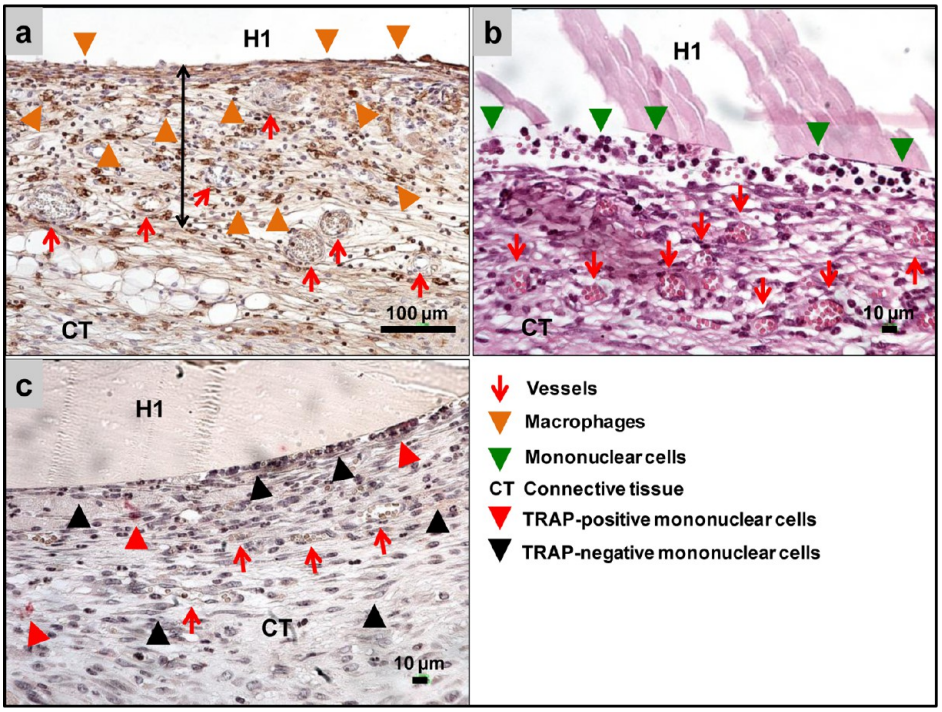

Figure 15. Tissue reaction to the H1 implant at day 10. (a) Macrophage-specific F4/80-immunostaining: an overview of the distribution of mononuclear cells within the peri-implant tissue (double arrow) within the subcutaneous (CT) layer of the CD1 mouse. Most of the cells at the surface as well as the periphery were identified as macrophages (orange arrowheads). (b) H&E staining: a granulation tissue was located at the surface of the implant. (c) TRAP staining: only a small amount of cells at the surface of the material as well as within the material-adherent tissue (CT) showed signs of TRAP activity (red arrowheads). Most of the cells were TRAP-negative (black arrowheads).

material induced two different cellular reactions. The bulk-like structures induced a mainly mononuclear inflammatory response, while the fragments induced multinucleated giant cells. The occurrence of the latter was independent of fragment size. Overall, the implantation bed of this group was relatively extensive, which again can be attributed to the presence of the multinucleated giant cells, which are known to produce vascular endothelial growth factor (VEGF) among other substances responsible for material degradation. H1 undergoes negligible fragmentation during the observation period, which can be attributed to its higher mechanical stability. This material induced mainly mononuclear cells and a relatively low amount of multinucleated giant cells. Interestingly, the latter did not show a high TRAP expression, and it was observed that the implantation bed of H1 was well vascularized.

CONCLUSIONS

PMMA–bioglass hybrids were produced by the sol–gel method in the presence of chemical bonding that integrated organic and inorganic components. This molecular level interaction addressed the issue of phase separation that is commonly observed in the preparation of physical mixtures of bioglass with a polymer. In addition, the mechanical properties of the hybrid acquired at an optimum composition of MPMA:MMA were significantly improved compared with bioglass; the Young's modulus of the hybrid was decreased 40-fold and its hardness was 16-fold higher than pure bioglass. The chemical bonding of PMMA with bioglass resulted in prolonging the degradation of bioglass, which may be favorable for bone regeneration and *in situ* drug release applications. Additionally, the results of *in vitro* and *in vivo* studies demonstrated that the molecular level interaction had no adverse effect on biocompatibility of bioglass and in fact significantly enhanced its integrity and reduced the level of inflammation. Therefore, the fabricated hybrid in this study is a viable alternative for bioglass and PMMA–bioglass physical mixtures as bone regenerative materials.

MATERIALS AND METHODS

Materials. Precursors required for the synthesis of PMMA-*co*-MPMA copolymer including MPMA, α,α′-azoisobutyronitrile (AIBN), and *N*,*N*′-dimethylformamide (DMF) were purchased from Sigma and used as received. Methyl methacrylate purchased from Sigma was used after distillation under reduced pressure. Hydrochloric acid (HCl; Merck), tetraethyl orthosilicate (TEOS; Sigma), calcium chloride dihydrate ($CaCl_2 \cdot 2H_2O$ (CC); Ajax Finechem Pty Ltd.), tetrahydrofuran (THF; Merck), and deionized water were used for fabrication of the inorganic solution and the hybrid.

Preparation of Bioglass, PMMA-*co*-MPMA, and Pure PMMA Solutions. TEOS was mixed with deionized water and HCl and stirred for 30 min followed by addition of calcium chloride dihydrate. A common calcium source for the preparation of sol−gel-derived bioglasses is calcium nitrate tetrahydrate; however, in this study, calcium chloride was used to minimize the risk of toxicity resulting from nitrate byproduct.[62] The precursors were mixed with a molar ratio of TEOS:water:HCl:CC = 1:8:0.01:0.2, and the solution is referred to as sol(A) for convenience.

A free radical polymerization technique was used for the synthesis of PMMA-*co*-MPMA with MPMA:MMA = 0.1 mol ratio coded as PMFS and PMMA (without MPMA) using AIBN as an initiator. Precursors were mixed in a Schlenk flask (MMA:AIBN = 200 (mol ratio), DMF (20 mL)) and degassed by three freeze−pump−thaw cycles. Polymerization was conducted at 70 °C for a period of 12 h. The polymer was purified by precipitation in diethyl ether followed by filtration and drying under vacuum. PMFS or PMMA was dissolved in THF with a concentration of 10 wt %, and the solutions were labeled as sol(B) and sol(C), respectively.

Hybrid Formation. Sol(A) and sol(B) were mixed in the volumetric ratio of sol(B):sol(A) = 60:40, then mechanically stirred for 1 h to obtain a homogeneous and well-dispersed solution. This composition was selected due to the fact that bioglass composition was shown to have no significant impact on the network characteristics and molecular integration of hybrids.

It was then kept sealed until a gel formed, then was dried at ambient temperature and subsequently at 37 °C for a period of 7 days at each temperature. The product was then dried in a vacuum oven at 40 °C for a period of 2 days. This temperature profile was developed for drying the samples to remove residues of solvents and maintain the monolith structure.

Physical Mixture Formation. Sol(A) and sol(C) were mixed (sol(C):sol(A) = 60:40 vol %) and mechanically stirred for 1 h. The same procedure was followed to dry these samples as hybrids. A thin film of polymer was obtained with a gel structure of bioglass, which was subsequently ground and well-mixed as a powder. After this, the powder was dissolved in THF (10 wt %) and cast on a Teflon container, which was then vacuum-dried at 40 °C for 2 days.

Characterizations. *Scanning Electron Microscopy−Energy Dispersive Spectrometry (SEM-EDS).* The surface microstructures and crystal phase formed on the specimens were analyzed by field emission scanning electron microscopy (FE-SEM; Zeiss ULTRA Plus). This instrument was equipped with a Bruker XFlash 4010 EDS detector with high-speed acquisition and hypermapping capability. Samples were mounted on aluminum stubs using conductive carbon paint, then gold coated by using an Emitech K7550X instrument prior to SEM analysis.

Scanning Transmission Electron Microscopy (STEM). STEM analysis was conducted to investigate the interaction between the phases in nanoscale. Samples were ground to powders, embedded in epoxy resins, and microtomed with Leica Ultracut ultramicrotomes (UC7) for 100 nm layers. The layers were harvested and seated on carbon grids prior to STEM analysis (Zeiss ULTRA Plus).

Atomic Force Microscopy (AFM). The surface topography of the prepared hybrid samples was characterized by an atomic force microscope (Asylum Research, MFP-3D-BIO) in ac mode using a silicon nitride tip (AC160). In order to identify the uniformity of distribution and separation of bioglass within the polymer structure, phase images were recorded. A thin film was produced to examine the surface properties.

Mechanical Testing. Hybrid samples were prepared in the form of monoliths, and uniaxial compression tests were performed in an unconfined state with a 1000 N load cell by Instron (model 5543). Dimensions of the samples were 6.61 ± 0.05 mm diameter and 1.2 ± 0.1 mm height. The samples were subjected to a loading, and a Young's modulus was obtained as the tangent slope of the stress−strain curve between 0% and 10% strain level. The area under the compressive stress−strain curves was calculated for measuring the toughness of the samples. Three samples were examined for each group for statistical analysis.

Microhardness measurements were performed using Vickers indentations at loads of 50 g and an indentation time of 5 s at 25 °C using a microhardness tester (Buehler, Lake Bluff, IL; 1105D). Six tests were conducted for each sample for statistical analysis.

Degradation Assessment. The degradation rate of samples was tested by measuring the change in sample weight over time under simulated physiological conditions. Three samples were kept in PBS at 37 °C, and at different time intervals they were removed from the degradation medium, rinsed three times with deionized water, and dried prior to weighing. The measurement was continued for a period of 100 days.

Attenuated Total Reflection Fourier Transform Infrared (ATR-FTIR) Spectroscopy. The molecular structure of the hybrid and the degradation products of samples after leaving in PBS for 100 days were analyzed by ATR-FTIR spectroscopy (FTIR; Nicolet 6700, Thermo Fisher Scientific Inc.). The samples were scanned at a speed of 32 scan/min.

Bioactivity. The samples were characterized for their bioactivity by incubation in simulated body fluid[63] at 37 °C for periods of 1, 3, 7, and 14 days. Samples were washed twice with deionized water to remove any residue of minerals absorbed on the surface. The dried monoliths were examined to determine the formation of an apatite layer on the surface.

Cell Attachment, Morphology, and Proliferation. Human preosteoblasts (HOB) were used to assess the cell interaction with the samples. Complete osteoblast growth media (Invitrogen) was used to culture the HOB cells, which were incubated at 37 °C in the presence of 5% CO_2 and 95% humidity. The media was refreshed every 3 days until the cells approached confluence.

The samples (12 mm diameter × 1 mm height) were placed into a well plate and kept in 70% ethanol for 1 h for sterilization, followed by rinsing with PBS three times. Samples were then exposed to UV light for 30 min and were washed with fresh medium at 37 °C overnight. The substrates were placed into well plates, seeded with cells at a density of 2×10^5 cells/mL, and kept in culture for 7 days. Cell morphology was examined at day 4 of culture by SEM (FE-SEM; Zeiss ULTRA plus) analysis after being fixed with glutaraldehyde according to a previously published method.[64] Viability was measured at 1 day and 7 days postseeding. Cellular viability was assessed using the CellTiter 96 Aqueous One Solution cell proliferation assay kit (Promega) according to the manufacturer's instructions. Briefly, scaffolds were incubated with the viability solution for 30 min at 37 °C and read using a spectrophotometer at 595 nm. All samples were analyzed triple for statistical analysis. Tissue culture polystyrene (TCPS) was used as a control.

In Vitro Osteogenic Differentiation and Alkaline Phosphatase Activity. To initiate osteogenic differentiation, samples were transferred to media supplemented with ascorbic acid (50 μg/mL), β-glycerophosphate (10 mM), and BMP-2 (200 ng/mL) after 48 h of culture with cells. The time of transferring the samples to this media was considered as day 0 for the alkaline phosphatase (ALP) test.

ALP is an osteogenic marker that is expressed by differentiating osteoblasts. ALP staining was carried out on pure PMMA and bioglass, their physical mixture, and hybrid at day 4. Samples were fixed with gluteraldehyde, washed with PBS, and incubated in TRIS buffer (1 M, 9.4 pH) for 5 min. The scaffolds were then stained in Naphthol AS-BI phosphate (Sigma) as a substrate and Fast Blue (Sigma) as the stain. Scaffolds were washed with H_2O to remove excess staining before imaging. Cells alone on tissue culture plastic were used as a control. Images were captured using a Leica MZ6 microscope with a QImaging Micropublisher 5.0 camera.

***In Vivo* Study.** *Experimental Design of the in Vivo Pilot Study.* The *in vivo* experiments were carried out after approval from the Committee on the Use of Live Animals in Teaching and Research of the State of Rhineland-Palatinate, Germany. A total of 10 female 4−6-week-old CD1-mice (Charles River Laboratories, Germany) were reared under standard experimental conditions at the *in vivo* Laboratory Animal Unit at the Institute of Pathology of the Johannes Gutenberg University of Mainz, Germany. The animals were randomly divided into three experimental groups. Animals of the first two groups (n = 4 and 8 animals in total) underwent a subcutaneous implantation with the bioglass and prepared hybrid in this study in accordance

with a previously described experimental setup.[65−72] Two additional animals (n = 2) underwent the preparation of the subcutaneous pocket without biomaterial insertion (control group). This control group served for classification of the inflammatory response related to the operation procedures.

Subcutaneous Implantation Model. The subcutaneous implantation of bone substitutes was applied according to a previously published operation procedure.[65−72] The animals were anesthetized with an intraperitoneal injection (10 mL of ketamine (50 mg mL^{-1}) with 1.6 mL of 2% xylazine). Subsequently, a subcutaneous pocket in the subscapular region was formed by means of a scalpel and surgical scissors. The bone substitute materials were subsequently inserted under sterile conditions into the subcutaneous tissue pocket under the thin skin muscle of the subscapular region. Wound closure was performed by means of Prolene 6.0 suture material (Ethicon, Germany).

Explantation and Tissue Preparation. The tissue preparation for all of the groups was performed according to a previously described method.[65−72] Experimental animals were sacrificed by an overdose of ketamine and xylazine at day 10 after implantation. After 10 days the bone substitute materials were resected together with the surrounding peri-implant tissue. Tissue fixation was carried out by means of 4% formalin for 24 h. For further histological workup and (immuno-) histochemical staining, the tissue of the implant site was cut into three segments of identical dimensions containing the left margin, the center, and the right margin of the biomaterial. Paraffin embedding was performed after dehydration of the biopsies in a series of increasing alcohol concentrations followed by xylol incubation. Six ongoing 3−5 μm thick sections were made from the central segment of each animal by means of a rotation microtome (Leica RM2255, Wetzlar, Germany).

Histological Examination of the Animal Tissue. The material−tissue interaction was visualized by means of previously published histochemical and immunohistochemical staining methods.[65−72] The first three slides sections were stained with hematoxylin and eosin (H&E), Movat's Pentachrome and Azan, respectively. The fourth slide was used to identify osteoclast-like cells by TRAP staining according to previously described methods. The fifth slide was used for immunochemical staining with a pan-macrophage marker (F4/80 antibody, rat monoclonal, Clon BM8, eBioScience, USA) in combination with peroxidase and diaminobenzidine (EnVision Detection System, peroxidase/DAB, rabbit/mouse, K5007; Dako Cytomation, Hamburg, Germany). The sixth slide served as a control of the staining method in absence of the F4/80 antibody. All of the other chemicals were purchased from Sigma-Aldrich and used without further purification.

Histological Analysis of Animal Tissues. The histopathological evaluation was performed by two independent investigators (S.G. and M.B.) by means of a conventional diagnostic microscope (Nikon Eclipse 80i, Tokyo, Japan). The description and the outcome of the cell− and tissue−biomaterial interactions were evaluated by examination of the total implantation bed and its peri-implant tissue as previously described.[65−72]

Statistical Analysis. Statistical significance was conducted by analysis of variance (ANOVA), and data were represented as mean ± standard deviation (SD). Statistical significance was indicated in the figures as *** (p < 0.001).

Conflict of Interest: The authors declare no competing financial interest.

Acknowledgment. The authors acknowledge the financial support from Australian Research Council. R.R. acknowledges the International Postgraduate Research Scholarship Award from the University of Sydney. The authors acknowledge the facilities and the scientific and technical assistance of the Australian Microscopy & Microanalysis Research Facility at the electron microscope unit, The University of Sydney.

REFERENCES AND NOTES

1. Chen, Q.; Roether J. A.; Boccaccini, A. R. Tissue Engineering Scaffolds from Bioactive Glass and Composite Materials. In *Topics In Tissue Engineering*; Ashammakhi, N., Reis, R., Chiellini, F., Eds.; 2008, http://www.oulu.fi/spareparts/ebook_topics_in_t_e_vol3/index.html.
2. Gerhardt, L.-C.; Boccaccini, A. R. Bioactive Glass and Glass-Ceramic Scaffolds for Bone Tissue Engineering. *Materials* **2010**, *3*, 3867–3910.
3. Jones, J. R.; Gentleman, E.; Polak, J. Bioactive Glass Scaffolds for Bone Regeneration. *Elements (Chantilly, VA, U. S.)* **2007**, *3*, 393–399.
4. Abou Neel, E. A.; Chrzanowski, W.; Valappil, S. P.; O'Dell, L. A.; Pickup, D. M.; Smith, M. E.; Newport, R. J.; Knowles, J. C. Doping of a High Calcium Oxide Metaphosphate Glass with Titanium Dioxide. *J. Non-Cryst. Solids* **2009**, *355*, 991–1000.
5. Abou, N. E. A.; Chrzanowski, W.; Georgiou, G.; Dalby, M. J.; Knowles, J. C. *In Vitro* Biocompatibility and Mechanical Performance of Titanium Doped High Calcium Oxide Metaphosphate-Based Glasses. *J. Tissue Eng.* **2010**, *1*, 1–11.
6. Misra, S. K.; Philip, S. E.; Chrzanowski, W.; Nazhat, S. N.; Roy, I.; Knowles, J. C.; Salih, V.; Boccaccini, A. R. Incorporation of Vitamin E in Poly(3hydroxybutyrate)/Bioglass Composite Films: Effect on Surface Properties and Cell Attachment. *J. R. Soc. Interface* **2009**, *6*, 401–409.
7. Rezwan, K.; Chen, Q. Z.; Blaker, J. J.; Boccaccini, A. R. Biodegradable and Bioactive Porous Polymer/Inorganic Composite Scaffolds for Bone Tissue Engineering. *Biomaterials* **2006**, *27*, 3413–3431.
8. Peltola, M. J.; Vallittu, P. K.; Vuorinen, V.; Aho, A. A. J.; Puntala, A.; Aitasalo, K. M. J. Novel Composite Implant in Craniofacial Bone Reconstruction. *Eur. Arch. Otorhinolaryngol.* **2012**, *269*, 623–628.
9. Song, X.; Wang, X.; Wang, H.; Zhong, W.; Du, Q. PMMA-Silica Hybrid Thin Films with Enhanced Thermal Properties Prepared *via* a Non-Hydrolytic Sol-Gel Process. *Mater. Chem. Phys.* **2008**, *109*, 143–147.
10. Kamimura, M.; Tamura, J.; Shinzato, S.; Kawanabe, K.; Neo, M.; Kokubo, T.; Nakamura, T. Bone-Bonding Strength of Two Kinds of Poly(methyl methacrylate)-Based Bioactive Bone Cement Containing Bioactive Glass Beads or Glass-Ceramic Powder. *Key Eng. Mater.* **2002**, *218−220*, 369–374.
11. Hamizah, A. S.; Mariatti, M.; Othman, R.; Kawashita, M.; Noor, H. A. R. Mechanical and Thermal Properties of Polymethylmethacrylate Bone Cement Composites Incorporated with Hydroxyapatite and Glass-Ceramic Fillers. *J. Appl. Polym. Sci.* **2012**, *125*, E661–E669.
12. Shinzato, S.; Nakamura, T.; Kokubo, T.; Kitamura, Y. PMMA-Based Bioactive Cement: Effect of Glass Bead Filler Content and Histological Change with Time. *J. Biomed. Mater. Res.* **2002**, *59*, 225–232.
13. Hautamaeki, M.; Meretoja, V. V.; Mattila, R. H.; Aho, A. J.; Vallittu, P. K. Osteoblast Response to Polymethyl Methacrylate Bioactive Glass Composite. *J. Mater. Sci.: Mater. Med.* **2010**, *21*, 1685–1692.
14. Jones, S. M.; Friberg, S. E.; Sjoblom, J. A Bioactive Composite Material Produced by the Sol-Gel Method. *J. Mater. Sci.* **1994**, *29*, 4075–4080.
15. Verne, E.; Miola, M.; Ferraris, S.; Masse, A.; Bistolfi, A.; Crova, M.; Maina, G. Composite Bone Cements with a PMMA Matrix, Containing Bioactive Antibacterial Glasses or Glass-Ceramics, PCT Int. Appl. WO2011004355A2, 2011.
16. Lee, K.-H.; Rhee, S.-H. The Mechanical Properties and Bioactivity of Poly(methyl methacrylate)/SiO_2-CaO Nanocomposite. *Biomaterials* **2009**, *30*, 3444–3449.
17. Orr, N. J. D. J. F. Measurement of Shrinkage Stresses in PMMA Bone Cement. *Appl. Mech. Mater.* **2004**, *1−2*, 127–132.
18. Kosuge, Y. Influence of PMMA Powder on Properties of MMA-TBB Resin Cement. *J. J. Soc. Dent. Mater. Dev.* **2000**, *19*, 92−101.
19. Charnley, J. Anchorage of the Femoral Head Prosthesis to the Shaft of the Femur. *J. Bone Joint Surg. Br.* **1960**, *42-B*, 28–30.
20. Endogan, T.; Serbetci, K.; Hasirci, N. Effects of Ingredients on Thermal and Mechanical Properties of Acrylic Bone Cements. *J. Appl. Polym. Sci.* **2009**, *113*, 4077–4084.
21. Ferreira, B. J. M. L.; Duarte, M. G. G. M.; Gil, M. H.; Correia, R. N.; Roman, J.; Vallet-Regi, M. *In Vitro* Bioactivity in Glass-Ceramic/PMMA-co-EHA Composites. *Key Eng. Mater.* **2004**, *254−256*, 581–584.

22. Vallo, C. I. Residual Monomer Content in Bone Cements Based on Poly(methyl methacrylate). *Polym. Int.* **2000**, *49*, 831–838.
23. Mousa, W. F.; Kobayashi, M.; Shinzato, S.; Kamimura, M.; Neo, M.; Yoshihara, S.; Nakamura, T. Biological and Mechanical Properties of PMMA-Based Bioactive Bone Cements. *Biomaterials* **2000**, *21*, 2137–2146.
24. Hasenwinkel, J. M.; Lautenschlager, E. P.; Wixson, R. L.; Gilbert, J. L. A Novel High-Viscosity, Two-Solution Acrylic Bone Cement: Effect of Chemical Composition on Properties. *J. Biomed. Mater. Res.* **1999**, *47*, 36–45.
25. Zulfikar, M. A.; Wahab, M. A.; Hilal, N. Preparation and Characterization of Novel Porous PMMA-SiO_2 Hybrid Membranes. *Desalination* **2006**, *192*, 262–270.
26. Chrzanowski, W.; Abou Neel, E. A.; Lee, K. Y.; Bismarck, A.; Young, A. M.; Hart, A. D.; Dalby, M. J.; Knowles, J. C. Tailoring Cell Behavior on Polymers by the Incorporation of Titanium Doped Phosphate Glass Filler. *Adv. Eng. Mater.* **2010**, *12*, B298–B308.
27. Guild, F. J.; Kinloch, A. J.; Taylor, A. C. Particle Cavitation in Rubber Toughened Epoxies: The Role of Particle Size. *J. Mater. Sci.* **2010**, *45*, 3882–3894.
28. Hsieh, T. H.; Kinloch, A. J.; Masania, K.; Sohn, L. J.; Taylor, A. C.; Sprenger, S. The Toughness of Epoxy Polymers and Fibre Composites Modified with Rubber Microparticles and Silica Nanoparticles. *J. Mater. Sci.* **2010**, *45*, 1193–1210.
29. Rhee, S.-H.; Choi, J.-Y. Preparation of a Bioactive Poly(methyl methacrylate)/Silica Nanocomposite. *J. Am. Ceram. Soc.* **2002**, *85*, 1318–1320.
30. Burdick, J. A.; Peterson, A. J.; Anseth, K. S. Conversion and Temperature Profiles during the Photoinitiated Polymerization of Thick Orthopedic Biomaterials. *Biomaterials* **2001**, *22*, 1779–1786.
31. Mammeri, F.; Le, B. E.; Rozes, L.; Sanchez, C. Mechanical Properties of Hybrid Organic-Inorganic Materials. *J. Mater. Chem* **2005**, *15*, 3787–3811.
32. Poologasundarampillai, G.; Ionescu, C.; Tsigkou, O.; Murugesan, M.; Hill, R. G.; Stevens, M. M.; Hanna, J. V.; Smith, M. E.; Jones, J. R. Synthesis of Bioactive Class II Poly(γ-Glutamic Acid)/Silica Hybrids for Bone Regeneration. *J. Mater. Chem.* **2010**, *20*, 8952–8961.
33. Mellon, V.; Rinaldi, D.; Bourgeat-Lami, E.; D'Agosto, F. Block Copolymers of γ-Methacryloxypropyltrimethoxysilane and Methyl Methacrylate by RAFT Polymerization. A New Class of Polymeric Precursors for the Sol-Gel Process. *Macromolecules* **2005**, *38*, 1591–1598.
34. Alvarado-Rivera, J.; Munoz-Saldana, J.; Ramirez-Bon, R. Nanoindentation Testing of SiO_2-PMMA Hybrid Films on Acrylic Substrates with Variable Coupling Agent Content. *J. Sol-Gel Sci. Technol.* **2010**, *54*, 312–318.
35. Avila-Herrera, C. A.; Gomez-Guzman, O.; Almaral-Sanchez, J. L.; Yanez-Limon, J. M.; Munoz-Saldana, J.; Ramirez-Bon, R. Mechanical and Thermal Properties of SiO_2-PMMA Monoliths. *J. Non-Cryst. Solids* **2006**, *352*, 3561–3566.
36. Chang, T. C.; Wang, Y. T.; Hong, Y. S.; Chiu, Y. S. Organic-Inorganic Hybrid Materials. V. Dynamics and Degradation of Poly(methyl methacrylate) Silica Hybrids. *J. Polym. Sci., Part A: Polym. Chem.* **2000**, *38*, 1972–1980.
37. Morales-Acosta, M. D.; Quevedo-Lopez, M. A.; Gnade, B. E.; Ramirez-Bon, R. PMMA-SiO_2 Organic-Inorganic Hybrid Films: Determination of Dielectric Characteristics. *J. Sol-Gel Sci. Technol.* **2011**, *58*, 218–224.
38. Yang, J.-M.; Lu, C.-S.; Hsuu, Y.-G.; Shih, C.-H. Mechanical Properties of Acrylic Bone Cement Containing PMMA-SiO_2 Hybrid Sol-Gel Material. *J. Biomed. Mater. Res.* **1997**, *38*, 143–154.
39. Liu, Q.; Ding, J.; Chambers, D. E.; Debnath, S.; Wunder, S. L.; Baran, G. R. Filler-Coupling Agent-Matrix Interactions in Silica/Polymethylmethacrylate Composites. *J. Biomed. Mater. Res.* **2001**, *57*, 384–393.
40. Wei, Y.; Jin, D.; Wei, G.; Yang, D.; Xu, J. Novel Organic-Inorganic Chemical Hybrid Fillers for Dental Composite Materials. *J. Appl. Polym. Sci.* **1998**, *70*, 1689–1699.
41. Rhee, S.-H.; Hwang, M.-H.; Choi, J.-Y. Effect of Silica Content in PMMA/Silica Hybrids Containing Calcium Salt on Calcium Phosphate Formation and Cell Responses. *Key Eng. Mater.* **2003**, *240–242*, 183–186.
42. Rhee, S.-H.; Hwang, M.-H.; Si, H.-J.; Choi, J.-Y. Biological Activities of Osteoblasts on Poly(methyl methacrylate)/Silica Hybrid Containing Calcium Salt. *Biomaterials* **2003**, *24*, 901–906.
43. Wei, Y.; Yang, D.; Bakthavatchalam, R. Thermal Stability and Hardness of New Polyacrylate-Silica Hybrid Sol-Gel Materials. *Mater. Lett.* **1992**, *13*, 261–266.
44. Ravarian, R.; Wei, H.; Rawal, A.; Hook, J.; Chrzanowski, W.; Dehghani, F. Molecular Interactions in Coupled PMMA-Bioglass Hybrid Networks. *J. Mater. Chem. B* **2013**, *1*, 1835–1845.
45. Mahony, O.; Tsigkou, O.; Ionescu, C.; Minelli, C.; Ling, L.; Hanly, R.; Smith, M. E.; Stevens, M. M.; Jones, J. R. Silica-Gelatin Hybrids with Tailorable Degradation and Mechanical Properties for Tissue Regeneration. *Adv. Funct. Mater.* **2010**, *20*, 3835–3845.
46. Martin, R. A.; Yue, S.; Hanna, J. V.; Lee, P. D.; Newport, R. J.; Smith, M. E.; Jones, J. R. Characterizing the Hierarchical Structures of Bioactive Sol-Gel Silicate Glass and Hybrid Scaffolds for Bone Regeneration. *Philos. Trans. R. Soc., A* **2012**, *370*, 1422–1443.
47. Colby, M. W.; Osaka, A.; Mackenzie, J. D. Effects of Temperature on Formation of Silica Gel. *J. Non-Cryst. Solids* **1986**, *82*, 37–41.
48. Zou, H.; Wu, S.; Shen, J. Polymer/Silica Nanocomposites: Preparation, Characterization, Properties, and Applications. *Chem. Rev. (Washington, DC, U. S.)* **2008**, *108*, 3893–3957.
49. Rho, J. Y.; Roy, M.; Pharr, G. M. Comments on 'Elastic Modulus and Hardness of Cortical and Trabecular Bone Lamellae Measured by Nanoindentation in the Human Femur'. *J Biomech.* **2000**, *33*, 1335–1337.
50. Ohman, C.; Baleani, M.; Perilli, E.; Dall'Ara, E.; Tassani, S.; Baruffaldi, F.; Viceconti, M. Mechanical Testing of Cancellous Bone from the Femoral Head: Experimental Errors Due to Off-Axis Measurements. *J. Biomech.* **2007**, *40*, 2426–2433.
51. Xu, C.; Su, P.; Chen, X.; Meng, Y.; Yu, W.; Xiang, A. P.; Wang, Y. Biocompatibility and Osteogenesis of Biomimetic Bioglass-Collagen-Phosphatidylserine Composite Scaffolds for Bone Tissue Engineering. *Biomaterials* **2010**, *32*, 1051–1058.
52. Puertolas, J. A.; Vadillo, J. L.; Sanchez-Salcedo, S.; Nieto, A.; Gomez-Barrena, E.; Vallet-Regi, M. Compression Behaviour of Biphasic Calcium Phosphate and Biphasic Calcium Phosphate-Agarose Scaffolds for Bone Regeneration. *Acta Biomater.* **2011**, *7*, 841–847.
53. Viitala, R.; Jokinen, M.; Rosenholm, J. B. Mechanistic Studies on Release of Large and Small Molecules from Biodegradable SiO_2. *Int. J. Pharm.* **2007**, *336*, 382–390.
54. Nieto, A.; Areva, S.; Wilson, T.; Viitala, R.; Vallet-Regi, M. Cell Viability in Wet Silica Gel. *Acta Biomater.* **2009**, *5*, 3478–3487.
55. Ahola, M. S.; Sailynoja, E. S.; Raitavuo, M. H.; Vaahtio, M. M.; Salonen, J. I.; Yli-Urpo, A. U. O. *In Vitro* Release of Heparin from Silica Xerogels. *Biomaterials* **2001**, *22*, 2163–2170.
56. Viitala, R.; Jokinen, M.; Maunu, S. L.; Jalonen, H.; Rosenholm, J. B. Chemical Characterization of Bio-Resorbable Sol-Gel Derived SiO_2 Matrices Prepared at Protein-Compatible pH. *J. Non-Cryst. Solids* **2005**, *351*, 3225–3234.
57. Poologasundarampillai, G.; Yu, B.; Tsigkou, O.; Valliant, E.; Yue, S.; Lee, P. D.; Hamilton, R. W.; Stevens, M. M.; Kasuga, T.; Jones, J. R. Bioactive Silica-Poly(γ-glutamic acid) Hybrids for Bone Regeneration: Effect of Covalent Coupling on Dissolution and Mechanical Properties and Fabrication of Porous Scaffolds. *Soft Matter* **2012**, *8*, 4822–4832.
58. De Aza, P. N.; Luklinska, Z. B.; Santos, C.; Guitian, F.; De, A. S. Mechanism of Bone-Like Formation on a Bioactive Implant *in Vivo*. *Biomaterials* **2003**, *24*, 1437–1445.
59. Kokubo, T.; Hanakawa, M.; Kawashita, M.; Minoda, M.; Beppu, T.; Miyamoto, T.; Nakamura, T. Apatite Formation on Non-Woven Fabric of Carboxymethylated Chitin in SBF. *Biomaterials* **2004**, *25*, 4485–4488.
60. Kokubo, T.; Takadama, H. How Useful Is SBF in Predicting *in Vivo* Bone Bioactivity? *Biomaterials* **2006**, *27*, 2907–2915.

61. Bohner, M.; Lemaitre, J. Can Bioactivity Be Tested *in Vitro* with SBF Solution? *Biomaterials* **2009**, *30*, 2175–2179.
62. Valliant, E. M.; Jones, J. R. Softening Bioactive Glass for Bone Regeneration: Sol-Gel Hybrid Materials. *Soft Matter* **2011**, *7*, 5083–5095.
63. Chrzanowski, W.; Yeow, W. J.; Rohanizadeh, R.; Dehghani, F. Bone Bonding Ability - How to Measure It? *RSC Adv.* **2012**, *2*, 9214–9223.
64. Zhong, X.; Dehghani, F. Fabrication of Biomimetic Poly-(propylene carbonate) Scaffolds by Using Carbon Dioxide as a Solvent, Monomer and Foaming Agent. *Green Chem.* **2012**, *14*, 2523–2533.
65. Ghanaati, S.; Barbeck, M.; Detsch, R.; Deisinger, U.; Hilbig, U.; Rausch, V.; Sader, R.; Unger, R. E.; Ziegler, G.; Kirkpatrick, C. J. The Chemical Composition of Synthetic Bone Substitutes Influences Tissue Reactions *in Vivo*: Histological and Histomorphometrical Analysis of the Cellular Inflammatory Response to Hydroxyapatite, Beta-Tricalcium Phosphate and Biphasic Calcium Phosphate Ceramics. *Biomed. Mater. (Bristol, U. K.)* **2012**, *7*, 015005/1–015005/14.
66. Ghanaati, S. M.; Thimm, B. W.; Unger, R. E.; Orth, C.; Kohler, T.; Barbeck, M.; Mueller, R.; Kirkpatrick, C. J. Collagen-Embedded Hdroxylapatite-Beta-Tricalcium Phosphate-Silicon Dioxide Bone Substitute Granules Assist Rapid Vascularization and Promote Cell Growth. *Biomed. Mater. (Bristol, U. K.)* **2010**, *5*, 025004/1–025004/11.
67. Ghanaati, S.; Schlee, M.; Webber, M. J.; Willershausen, I.; Barbeck, M.; Balic, E.; Goerlach, C.; Stupp, S. I.; Sader, R. A.; Kirkpatrick, C. J. Evaluation of the Tissue Reaction to a New Bilayered Collagen Matrix *in Vivo* and Its Translation to the Clinic. *Biomed. Mater. (Bristol, U. K.)* **2011**, *6*, 015010/1–015010/12.
68. Ghanaati, S.; Orth, C.; Unger, R. E.; Barbeck, M.; Webber, M. J.; Motta, A.; Migliaresi, C.; Kirkpatrick, C. J. Fine-Tuning Scaffolds for Tissue Regeneration: Effects of Formic Acid Processing on Tissue Reaction to Silk Fibroin. *J. Tissue Eng. Regener. Med.* **2010**, *4*, 464–472.
69. Ghanaati, S.; Orth, C.; Barbeck, M.; Willershausen, I.; Thimm, B. W.; Booms, P.; Stuebinger, S.; Landes, C.; Sader, R. A.; Kirkpatrick, C. J. Histological and Histomorphometrical Analysis of a Silica Matrix Embedded Nanocrystalline Hydroxyapatite Bone Substitute Using the Subcutaneous Implantation Model in Wistar Rats. *Biomed. Mater. (Bristol, U. K.)* **2010**, *5*, 035005/1–035005/11.
70. Ghanaati, S.; Barbeck, M.; Orth, C.; Willershausen, I.; Thimm, B. W.; Hoffmann, C.; Rasic, A.; Sader, R. A.; Unger, R. E.; Peters, F.; Kirkpatrick, C. J. Influence of β-Tricalcium Phosphate Granule Size and Morphology on Tissue Reaction *in Vivo*. *Acta Biomater.* **2010**, *6*, 4476–4487.
71. Ghanaati, S.; Barbeck, M.; Hilbig, U.; Hoffmann, C.; Unger, R. E.; Sader, R. A.; Peters, F.; Kirkpatrick, C. J. An Injectable Bone Substitute Composed of Beta-Tricalcium Phosphate Granules, Methylcellulose and Hyaluronic Acid Inhibits Connective Tissue Influx Into Its Implantation Bed *in Vivo*. *Acta Biomater.* **2011**, *7*, 4018–4028.
72. Ghanaati, S. Non-Cross-Linked Porcine-Based Collagen I-III Membranes Do Not Require High Vascularization Rates for Their Integration within the Implantation Bed: A Paradigm Shift. *Acta Biomater.* **2012**, *8*, 3061–3072.